Acta Crystallographica Section A
Foundations of Crystallography
ISSN 0108-7673

Received 7 February 2012
Accepted 26 June 2012

Experimental dynamic electron densities of multipole models at different temperatures

Swastik Mondal, Siriyara Jagannatha Prathapa and Sander van Smaalen*

Laboratory of Crystallography, University of Bayreuth, 95440 Bayreuth, Germany. Correspondence e-mail: smash@uni-bayreuth.de

It is shown that the dynamic electron density corresponding to a structure model can be computed by inverse Fourier transform of accurately calculated structure factors, employing the method of fast Fourier transform. Maps free of series-termination effects are obtained for resolutions better than 0.04 Å in direct space, corresponding to resolutions larger than 6 $Å^{-1}$ in reciprocal space. Multipole (MP) models of α-glycine and D,L-serine at different temperatures have been determined by refinement against X-ray diffraction data obtained from the scientific literature. The successful construction of dynamic electron densities is demonstrated by their topological properties, which indicate local maxima and bond-critical points (BCPs) at positions expected on the basis of the corresponding static electron densities, while non-atomic maxima have not been found. Density values near atomic maxima are much smaller in dynamic than in static electron densities. Static and low-temperature ($\sim$20 K) dynamic electron-density maps are found to be surprisingly similar in the low-density regions. Especially at BCPs, values of the $\sim$20 K dynamic density maps are only slightly smaller than values of the corresponding static density maps. The major effect of these zero-point vibrations is a modification of the second derivatives of the density, which is most pronounced for values at the BCPs of polar C—O bonds. Nevertheless, dynamic MP electron densities provide an estimate of reasonable accuracy for the topological properties at BCPs of the corresponding static electron densities. The difference between static and dynamic electron densities increases with increasing temperature. These differences might provide information on temperature-dependent molecular or solid-state properties like chemical stability and reactivity. In regions of still lower densities, like in hydrogen bonds, static and dynamic electron densities have similar appearances within the complete range of temperatures that have been considered (20–298 K), providing similar values of both the density and its Laplacian at BCPs in static and dynamic electron densities at all temperatures.

1. Introduction

Electron-density studies of molecular materials have been rationalized by the advent of the *quantum theory of atoms in molecules* (QTAIM) (Bader, 1990; Matta & Boyd, 2007). One fundamental aspect of the QTAIM is that it is only defined for static electron densities. As a consequence, the analysis of deconvoluted static densities has become prevalent in the field of experimental electron-density studies (Coppens & Volkov, 2004). Based on the static electron densities obtained from an experimental multipole (MP) model, information on chemical interactions and chemical properties can be retrieved with the aid of the QTAIM.

On the other hand, chemical interactions depend on temperature, as is illustrated by the ubiquitous occurrence of temperature-dependent phase transitions between different crystalline states of a single compound. One way to take into account the effects of temperature is the consideration of time-averaged electron densities, denoted as dynamic electron densities. In fact, the intensities of Bragg reflections measured in X-ray diffraction experiments directly reflect the dynamic electron density. It is only through a structure model that the static density and thermal vibrations can be deconvoluted (Hirshfeld, 1976; Coppens, 1997). The analysis of dynamic electron densities in association with the corresponding static electron density may thus be helpful in revealing the effects of temperature on chemical interactions and properties.

Dynamic electron densities corresponding to a structure model are defined as the convolution of the static electron density with the probability distribution functions of the atomic positions – where the latter follow from the thermal parameters. A direct numerical evaluation of this convolution product is too resource intensive, while a tractable analytical expression does not exist for cases in which the static density is

described by the MP model (Roversi *et al.*, 1998). Instead, dynamic electron densities can be computed by inverse Fourier transform of the structure factors of the structure model (Coppens, 1997). However, electron densities obtained by inverse Fourier transform of the structure factors suffer from series-termination effects, unless all reflections are included in the Fourier summation up to a resolution much higher than any resolution that can be achieved experimentally (de Vries, Briels, Feil *et al.*, 1996; de Vries, Briels & Feil, 1996). In a different approach, Roversi *et al.* (1998) have demonstrated that structure factors of high-order reflections can be added to the structure factors of low-order reflections, thereby compensating for the series-termination effects in a so-called anti-aliasing procedure.

Despite their potential, these methods have not been applied to MP models. One reason is that the computation of the structure factors for so many reflections has become feasible only in recent years with the increase of available computational power. Earlier work has concentrated on dynamic electron densities or dynamic deformation densities as obtained by inverse Fourier transform of a limited set of structure factors (Ruysink & Vos, 1974; Stevens *et al.*, 1977; Nijveldt & Vos, 1988; Coppens, 1997; Jelsch *et al.*, 1998; Coppens & Volkov, 2004). A qualitative analysis of these maps has shown that the dynamic density near nuclei is lower than the corresponding static density, and that the accumulation of charge in covalent bonds in static densities is retained in the dynamic densities. However, a quantitative analysis of the topological properties of these dynamic electron densities has not been achieved, mainly due to the presence of series-termination effects in the calculated maps (Stevens *et al.*, 1977; Jelsch *et al.*, 1998). Since experimental dynamic density maps with series-termination effects were not suitable for comparison with the theoretical maps, Stevens *et al.* (1977) have proposed to include a comparable amount of series-termination effects in the theory. However, any further development in this direction has not been found in the literature. A quantitative description of the effect of temperature on the density is of interest especially in the bonding region and at bond-critical points (BCPs), because these regions define the chemical interactions.

Here we present a method of computing dynamic electron densities corresponding to structure models, including independent atom models (IAM) and MP models. The method comprises an inverse Fourier transform by the method of fast Fourier transform (FFT) of accurately computed structure factors up to very high resolution. It is applied to two amino acids, α-glycine and D,L-serine (Figs. 1 and 2), for which low-temperature, high-resolution X-ray diffraction data are available from the literature (Destro *et al.*, 2000; Dittrich *et al.*, 2005).

Diffraction data at ~20 K for both compounds have allowed us to establish quantitatively the effects of zero-point vibrations on the electron densities, with the result that topological properties at BCPs are surprisingly similar between static and dynamic densities. The main difference is a reduction of the magnitudes of Laplacians.

In this respect it should be noticed that, unlike the QTAIM for static densities, a theoretical foundation does not exist for the interpretation of topological properties of dynamic electron densities. Instead, theoretical approaches accounting for the effects of temperature on properties retain the Born–Oppenheimer approximation for calculating the electronic structure, but combine this with different geometrical arrangements of the atoms, as obtained, for example, in the 'frozen phonon' approach or from molecular dynamics in the Car–Parrinello method (Car & Parrinello, 1985). The Car–Parrinello method has been applied to investigate the influence of temperature on molecular structure and properties (Cavazzoni *et al.*, 2002; Cyrański *et al.*, 2008; Gaigeot, 2008).

From these methods one could compute a time-averaged theoretical electron density, but such an approach would depend on an exact knowledge of the vibrational motion of the atoms, which is usually not available.

In the absence of a theoretical foundation for interpreting dynamic charge densities, we have performed a comparative

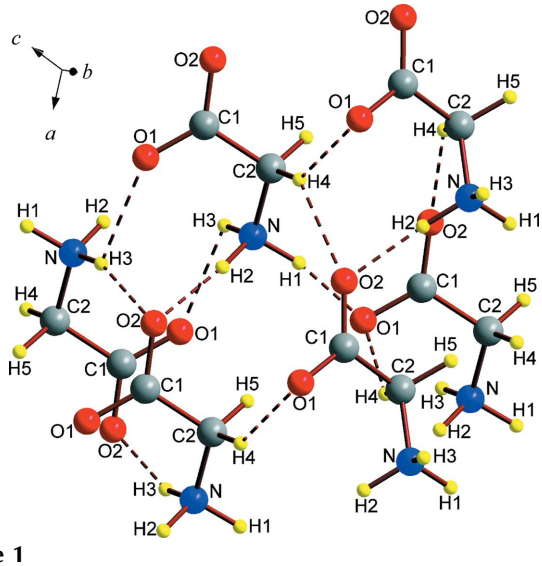

Figure 1
A perspective view of the crystal structure of α-glycine along with the atom-numbering scheme. Hydrogen bonds are shown as dashed lines.

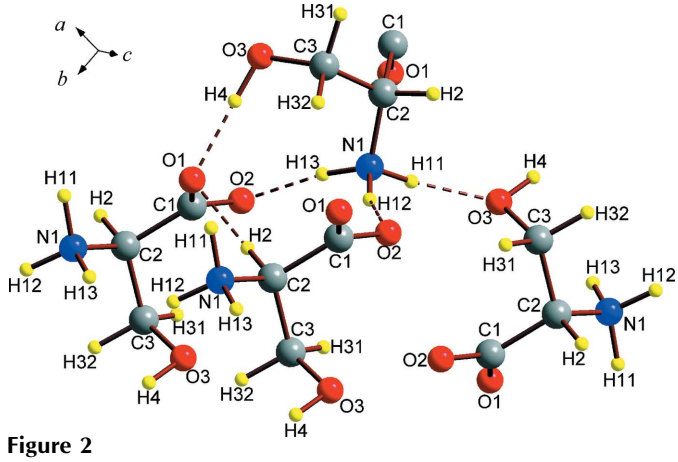

Figure 2
A perspective view of D,L-serine including hydrogen bonds along with the atom-numbering scheme.

topological analysis of static and dynamic electron densities of α-glycine and D,L-serine. The results provide an empirical description of the differences and similarities of these two entities. The effect of temperature on the dynamic charge density is studied by analysing diffraction data of D,L-serine measured at temperatures of 20, 100 and 298 K (Dittrich *et al.*, 2005).

2. The dynamic electron density

2.1. Method

The time-averaged electron density of a crystal with $N_{\rm atom}$ atoms in the unit cell is defined as

$$\langle\rho(\mathbf{r})\rangle = \sum_{\mathbf{L}}^{\rm volume}\sum_{\mu=1}^{N_{\rm atom}}\int \rho_\mu(\mathbf{r}-\mathbf{L}-\mathbf{r}_\mu^0-\mathbf{u}_\mu)P(\mathbf{u}_\mu)\,{\rm d}\mathbf{u}_\mu, \quad (1)$$

where $\rho_\mu(\mathbf{r}-\mathbf{L}-\mathbf{r}_\mu^0-\mathbf{u}_\mu)$ is the static electron density of atom μ located at $(\mathbf{r}_\mu^0+\mathbf{u}_\mu)$ in unit cell $\mathbf{L}$; $P(\mathbf{u}_\mu)$ is the probability of finding atom μ at position $\mathbf{r}_\mu^0+\mathbf{u}_\mu$; and $\mathbf{r}_\mu^0$ is the equilibrium position of atom μ. The Fourier transform of equation (1) defines the structure factors of the model. Within the harmonic approximation of lattice vibrations, the structure factor has the form

$$F(\mathbf{H}) = \sum_{\mu=1}^{N_{\rm atom}} f_\mu(\mathbf{H})\exp\left(-2\pi^2\,\mathbf{H}^T\mathbf{U}_\mu\mathbf{H}\right)\,\exp\left(2\pi i\,\mathbf{H}\cdot\mathbf{r}_\mu^0\right), \quad (2)$$

where $f_\mu(\mathbf{H})$ is the aspherical atomic scattering factor of atom μ, including contributions of any multipole functions; $\mathbf{U}_\mu$ is the tensor of the atomic displacement parameters (ADPs); and $\mathbf{H}$ is a reciprocal-lattice vector with indices (hkl) defined by

$$\mathbf{H} = h\mathbf{a}^* + k\mathbf{b}^* + l\mathbf{c}^*. \quad (3)$$

$\mathbf{H}^T$ is the transpose of the vector $\mathbf{H}$. The electron density can be obtained by inverse Fourier transform of the structure factors according to

$$\rho(\mathbf{r}) = \frac{1}{V_{\rm cell}}\sum_{j=1}^{N_{\rm refl}} F\left(\mathbf{H}_j\right)\,\exp\left(-2\pi i\,\mathbf{H}_j\cdot\mathbf{r}\right), \quad (4)$$

where $V_{\rm cell}$ is the volume of the unit cell and the summation runs over all reflections up to a desired resolution.

The electron density is obtained from the structure factors according to equation (4) by FFT. For this purpose, the electron density is defined on a grid of $N_{\rm pix} = N_1 \times N_2 \times N_3$ pixels. In reciprocal space this allows the storage of structure factors with indices up to $h_{\rm max} \simeq N_1/2$, $k_{\rm max} \simeq N_2/2$ and $l_{\rm max} \simeq N_3/2$. The mesh of sampling the density is given by the grid size of a/N_1 along $\mathbf{a}$, and similarly along $\mathbf{b}$ and $\mathbf{c}$. Hence, the relationship between the maximum resolution of the reflections and the grid size is

$$\left[\frac{\sin(\theta)}{\lambda}\right]_{\rm max} \simeq \frac{0.25}{\text{grid size}}. \quad (5)$$

For example, for a grid size of 0.04 Å, the resolution of the reflections that can be taken into account in the Fourier summation is $[\sin(\theta)/\lambda]_{\rm max} \simeq 6.25$ Å^{-1}.

Experimentally, structure factors are typically available up to resolutions of 1.3 Å^{-1} or worse. However, the structure factors of a structure model can be computed up to any resolution. This task has been implemented for the MP model in the latest version of the computer program *PRIOR* (see Appendix *A*), which also provides a code for computing the inverse Fourier transform [equation (4)] (van Smaalen *et al.*, 2003). The same code can be used to compute the dynamic electron density of the IAM, if MP parameters are set to zero.

2.2. Computational details

Dynamic electron densities of α-glycine at 23 K and of D,L-serine at 20, 100 and 298 K have been computed by inverse FFT of the model structure factors, employing the modified version of the computer program *PRIOR* (Appendix *A*). Different grid sizes have been employed for the dynamic electron density of α-glycine, while for D,L-serine the calculations have been restricted to the optimal grid size of 0.04 Å (Table 1 and §4). In each case, all structure factors have been included in the FFT, which can be stored on the chosen grid. Dynamic electron densities have been calculated both for the MP model and the corresponding IAM model.

In the present context, dynamic deformation densities are defined as the difference between the dynamic density of an MP model and the dynamic density of the corresponding IAM:

$$\Delta\rho_{\rm MP}^{\rm dyn-def}(\mathbf{r}) = \rho_{\rm MP}^{\rm dynamic}(\mathbf{r}) - \rho_{\rm IAM}^{\rm dynamic}(\mathbf{r}). \quad (6)$$

Dynamic deformation densities have been computed by a simple computer program, which subtracts the two relevant densities on a pixel-by-pixel basis.

Static electron densities and static deformation densities have been visualized by contour maps emphasizing the regions of low density. They have been generated by the module *XDGRAPH* of the program *XD2006* (Volkov *et al.*, 2006). Contour maps of dynamic densities and dynamic deformation densities have been generated with the computer program *JANA2006* (Petricek *et al.*, 2006).

Topological properties of static densities have been calculated with *XDPROP* (Volkov *et al.*, 2006). Topological properties of dynamic charge densities have been calculated with the latest version of the computer program *EDMA* (Palatinus *et al.*, 2012).

3. Choice of the aspherical model

There are different multipolar formalisms established in the literature. For α-glycine, Destro *et al.* (2000) have used the formalism of Stewart (1976) as implemented in the computer program *VALRAY* (Stewart & Spackman, 1983). For D,L-serine, Dittrich *et al.* (2005) have used an invariom model (Dittrich *et al.*, 2004) within the Hansen and Coppens formalism (Coppens, 1997). In order to have a consistent approach, we have decided to employ a single formalism and single procedure for obtaining the aspherical structure models of both compounds. For this, we have chosen the multipolar

Table 1
Crystallographic data for α-glycine at 23 K and for D,L-serine at 20, 100 and 298 K.

	α-Glycine, 23 K†	D,L-Serine, 20 K‡	D,L-Serine, 100 K‡	D,L-Serine, 298 K‡
Chemical formula	$C_2H_5NO_2$	$C_3H_7NO_3$	$C_3H_7NO_3$	$C_3H_7NO_3$
Temperature (K)	23	20	100	298
Crystal system	Monoclinic	Monoclinic	Monoclinic	Monoclinic
Space group	$P2_1/n$	$P2_1/a$	$P2_1/a$	$P2_1/a$
Z	4	4	4	4
a (Å)	5.0866	10.7764	10.7621	10.7355
b (Å)	11.7731	9.1947	9.1771	9.1456
c (Å)	5.4595	4.7788	4.7883	4.8304
α, β, γ (°)	90, 111.99, 90	90, 106.87, 90	90, 106.76, 90	90, 106.46, 90
V (Å^3)	303.16	453.13	452.82	454.83
$F(000)$	160	224	224	224
Wavelength (Å)	0.7107	0.7107	0.7107	0.7107
$(\sin\theta/\lambda)_{max}$ (Å^{-1})	1.15	1.18	1.19	0.98
Observed criteria	$F > 3\sigma_F$	$F > 4\sigma_F$	$F > 4\sigma_F$	$F > 4\sigma_F$
Number of unique reflections (obs/all)	3603/3822	4288/5136	4101/5146	2707/3551
Multipole refinement§				
R_F (obs/all)	0.0124/0.0145	0.0176/0.0253	0.0206/0.0326	0.0211/0.0335
wR_{F^2} (obs)	0.0293	0.0398	0.0434	0.0489
Goodness of fit	1.18	1.17	1.13	1.28
$\Delta\rho_{min}/\Delta\rho_{max}$ (e Å^{-3})	−0.132/0.154	−0.224/0.210	−0.210/0.207	−0.194/0.228
Dynamic density§				
Approximate pixel size (Å)	0.04	0.04	0.04	0.04
No. of pixels	128 × 288 × 144	256 × 216 × 128	256 × 216 × 128	256 × 216 × 128

† X-ray diffraction data from Destro *et al.* (2000). ‡ X-ray diffraction data from Dittrich *et al.* (2005). § Present work.

formalism of Hansen and Coppens (Coppens, 1997) as implemented in the computer program *XD2006* (Volkov *et al.*, 2006). During the process of developing an MP model with *XD2006*, we have failed to exactly reproduce the model of Destro *et al.* (2000) (see supplementary material for details[1]). The differences between the present model and that of Destro *et al.* (2000) can be attributed to the use of different multipolar formalisms, different software and different atomic scattering factors. We do not concentrate further on reproducing previous results since our results are very similar to those for other amino acids, including those from Destro *et al.* (2000), and the observed differences fall within the range of experimental values reported for amino acids (Mebs *et al.*, 2006). We have chosen the procedure that is the state of the art for performing multipole refinements using the software *XD2006*.

3.1. Multipole refinement of α-glycine

A strategic refinement according to the IAM has been performed by the computer program *SHELXL97* (Sheldrick, 2008) under the *WinGX* (Farrugia, 1999) software package. High-order data ($d \leq 0.50$ Å) have been used for refining the coordinates and ADPs of the non-H atoms, and they were kept fixed afterwards. Low-order data ($d \geq 1.0$ Å) have been used for refining coordinates of H atoms. U_{iso} of H atoms have been taken as $1.2 \times U_{eq}$ of their parent atoms. The resulting structure model was then introduced into the program *XD2006* (Volkov *et al.*, 2006) by the *XDINI* module. Atomic scattering factors have been taken from Su & Coppens (1998). In accordance with the environments of the atoms in α-glycine, local threefold symmetry (3) has been applied to the MP parameters of the N atom, and local mirror symmetry (m) has been applied to the MP parameters of all other non-H atoms (C1, C2, O1 and O2), which form the planar skeleton of the amino acid (Fig. 1). For non-H atoms, only those multipoles ($l_{max} = 4$) have been refined that are allowed by the local symmetry. Different κ and κ' parameters have been assigned to different atoms, depending on their chemical environment. For H atoms, fixed values of $\kappa = 1.10$ and $\kappa' = 1.18$ have been used. Only bond-directed multipoles truncated at the quadrupole level have been used for H atoms. All H atoms were initially set to neutron distances, subsequently refined against low-order data [$\sin(\theta)/\lambda \leq 0.5$ Å^{-1}] and then fixed to neutron distances again. The function minimized during least-square refinements is $\sum[w|F_o| - k|F_c|]^2$ with a weight of $1/\sigma^2[F_o]$ (Table 1).

3.2. Multipole refinement of D,L-serine

Dittrich *et al.* (2005) have used the invariom model – containing MP parameters determined by quantum chemical calculations (Dittrich *et al.*, 2004) – for all three data sets of D,L-serine. To be more experimentally oriented, we have decided to perform a complete multipole refinement for the 20 K data. However, for the structure refinements against data sets measured at 100 and 298 K, we have fixed the values of the MP parameters to those determined at 20 K. In this respect it should be noticed that the 298 K data are unsuitable for an *ab initio* MP refinement. The use of fixed MP parameters will contribute to our understanding, whether or not the present procedure for computing dynamic electron-density distributions is extendable to so-called normal data sets, where *ab initio* MP refinement is not possible.

[1] Supplementary material for this paper is available from the IUCr electronic archives (Reference: KX5007). Services for accessing these data are described at the back of the journal.

Table 2
Properties of dynamic electron densities of α-glycine at 23 K for various grid sizes.

Grid size (Å)	No. of pixels	$[\sin(\theta)/\lambda]_{max}$ (Å^{-1})	d_{min} (Å)	ρ_{min} (e Å^{-3})	ρ_{max} (e Å^{-3})
0.01	512 × 1152 × 576	25.000	0.02	0.0065	153.6673
0.02	256 × 576 × 288	12.500	0.04	0.0065	153.4111
0.04	128 × 288 × 144	6.250	0.08	0.0065	152.0316
0.05	96 × 216 × 108	5.000	0.10	0.0065	146.4684
0.07	72 × 162 × 72	3.571	0.14	0.0030	148.7689
0.08	64 × 144 × 72	3.125	0.16	−0.0284	138.2838
0.1	48 × 108 × 54	2.500	0.20	−0.3577	127.1692

Table 3
Electron densities (e Å^{-3}; first line) and Laplacians (e Å^{-5}; second line) at the BCPs of covalent bonds of the dynamic multipole densities of α-glycine at four grid sizes.

	Grid size (Å)			
Bond	0.01	0.02	0.04	0.05
C1—O1	2.701	2.701	2.701	2.701
	−19.45	−19.44	−19.44	−19.46
C1—O2	2.648	2.648	2.648	2.649
	−23.63	−23.63	−23.61	−22.95
C1—C2	1.698	1.698	1.698	1.698
	−13.28	−13.28	−13.28	−13.66
C2—N	1.657	1.657	1.657	1.657
	−10.22	−10.22	−10.21	−10.21

The feasibility of obtaining electron densities from such data sets has recently been studied by Dittrich *et al.* (2009) by initially using an invariom model to obtain ADPs followed by the refinement of the MP parameters.

The MP refinement at 20 K has been performed following the same strategy as we have used for α-glycine (Table 1 and Fig. 2).

4. Establishing the grid size

Electron densities obtained by means of the FFT may suffer from series-termination effects (§1). The grid size in direct space is directly related to the number of structure factors that can be incorporated into the Fourier summation [equation (5)]. Therefore, the dependence of series-termination effects on the grid size has been determined by calculations of the dynamic electron densities of α-glycine for seven different grid sizes (Table 2).

Ripples in the neighbourhood of a BCP are visible in the dynamic electron densities computed with grid sizes larger than 0.05 Å (Fig. 3). For a grid size of 0.07 Å, these ripples prevent a meaningful definition of the BCP and its properties. For a grid size of 0.08 Å the amplitude of the ripples is so large that negative density values are found at some points, a feature that is obviously unphysical.

Ripples in the electron densities have not been found for grid sizes of 0.05 Å and below. The dynamic electron densities are essentially the same when calculated with grid sizes of 0.04 and 0.02 Å. The contours of equal density appear smooth in these maps at any density level. For a grid size of 0.05 Å, the map does not suffer from ripples, but the shapes of the contours are slightly different from the maps at better resolutions, and the contours of low density are not perfectly smooth (Fig. 3). These observations suggest that a grid size of 0.04 Å or better is sufficient and necessary for computation of a dynamic charge density free of series-termination effects.

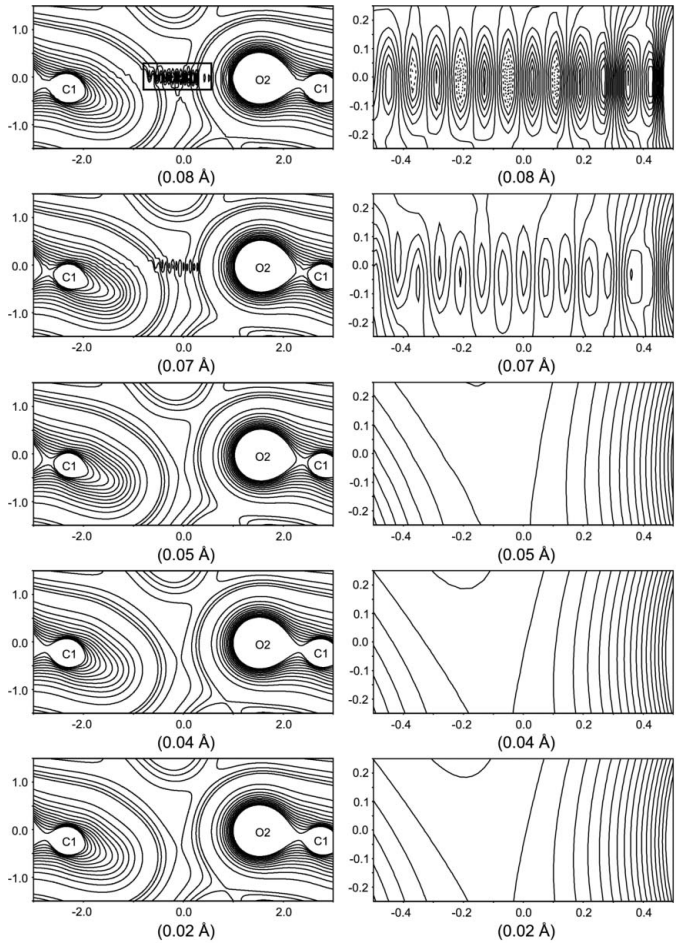

Figure 3
Effect of the grid size on the dynamic electron density of α-glycine. Left column: cross section of the dynamic electron density in the plane in which the maximum series-termination effect occurs. Contour lines are at an interval of 0.02 e Å^{-3} from 0 to 0.1 e Å^{-3} and at an interval of 0.2 e Å^{-3} from 0.1 to 2.5 e Å^{-3}. Right column: expanded view of the region marked by the rectangle in the top left map, which contains series-termination ripples. Contour lines are at an interval of 0.01 e Å^{-3} from 0.0 to 0.2 e Å^{-3}.

Series-termination effects are also apparent from the minimum values of the electron densities obtained at various resolutions, converging to a small positive value for grid sizes better than 0.05 Å (Table 2), again suggesting that the maps at resolutions of 0.04 Å or better are essentially the same. A true convergence is not achieved for the dependence on grid size of the maximum density (Table 2). This is explained by the spiky nature of the maximum, while smaller grid sizes mean that the density at the maximum is averaged over the smaller volume of a single voxel, thus leading to a larger value. Values of topological properties at the BCPs of the dynamic electron densities are identical for grid sizes of 0.01, 0.02 and 0.04 Å,

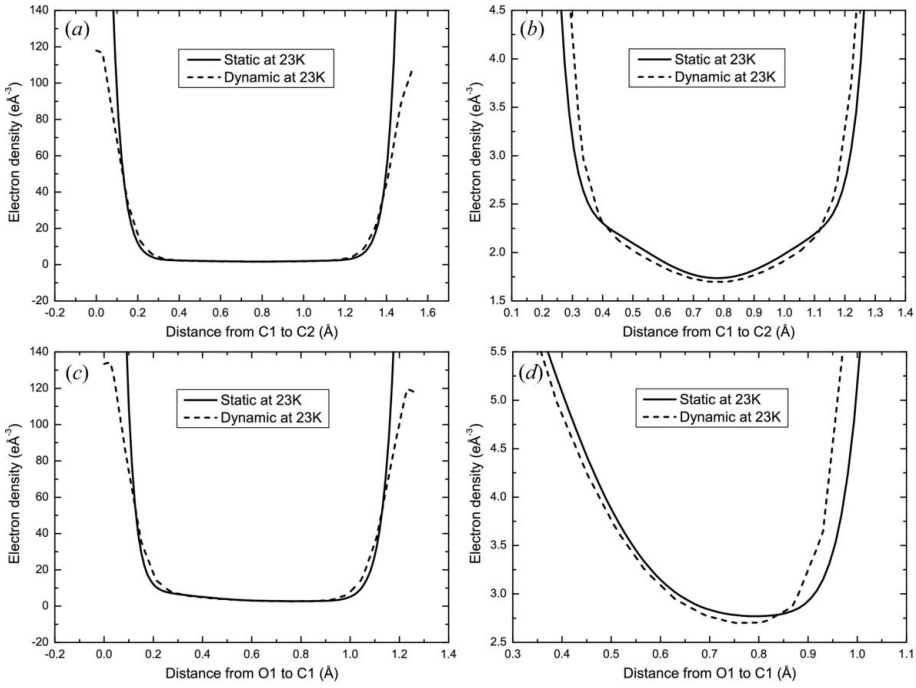

Figure 4
Distribution of static and dynamic MP electron densities of α-glycine *versus* distance from nuclei along bond paths. (*a*) Electron-density distribution along the bond path C1—C2. Static densities close to nuclei are truncated at 140 e Å^{-3}. (*b*) Electron densities are scaled up to show details of electron-density distribution near the BCP of C1—C2. (*c*) Electron-density distribution along the bond path O1—C1. Static densities close to nuclei are not shown. (*d*) Static and dynamic electron densities along O1—C1; densities are scaled up near the BCP of O1—C1.

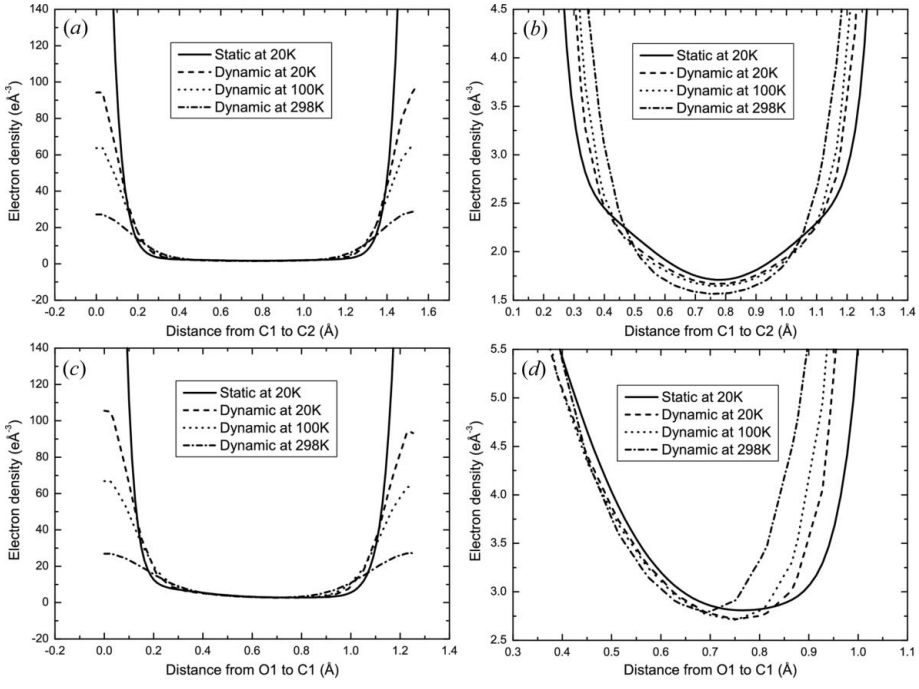

Figure 5
Distribution of static and dynamic MP densities of D,L-serine *versus* distance from nuclei along bond paths. (*a*) Electron-density distribution along the bond path C1—C2. Static densities close to nuclei are not shown. (*b*) Expanded view of (*a*), showing details of the variations of the electron densities near the BCP. (*c*) Electron-density distribution along the bond path O1—C1. Static densities close to nuclei are excluded. (*d*) Expanded view of (*c*), showing details of the variations of the electron densities near the BCP.

while they are slightly different from these values for a grid size of 0.05 Å (Table 3).

All these results indicate the absence of series-termination effects in dynamic charge densities computed with grid sizes of 0.04 Å and below. Therefore, we have chosen a grid size of 0.04 Å as the optimum grid size for the computation of dynamic electron densities by inverse FFT of the structure factors. The corresponding resolution of the structure factors is $[\sin(\theta)/\lambda]_{\max} \simeq 6.25$ Å^{-1} [equation (5)]. This resolution is similar to the resolution of 5.5 Å^{-1} proposed by de Vries, Briels & Feil (1996) and to the resolution of 6 Å^{-1} proposed by Roversi *et al.* (1998). The grid size of 0.04 Å also falls within the range (0.025–0.05 Å) suitable for precise calculation of topological properties of electron densities as suggested earlier in the literature (Katan *et al.*, 2003; Rabiller *et al.*, 2004; Palatinus *et al.*, 2012).

The present results clearly demonstrate the need to include weak reflections in the Fourier summations, with resolutions far beyond those that can be reached in a diffraction experiment. The computation of static electron densities by inverse FFT of the structure factors (ADPs are equal to zero) failed to converge to maps free of series-termination effects, down to grid sizes of 0.01 Å. This can be understood from the form of the atomic form factors, which have a simple exponential dependence on the distance to the nucleus for large distances (Coppens, 1997). The Debye–Waller factor represents a Gaussian distribution at large distances, which goes to zero much faster than the exponential dependence. Apparently, the exponential dependence is insufficiently fast to allow high-order structure factors to be neglected. In direct space, this failure demonstrates that any resolution of reflections will be insufficient for describing the spikes in the static electron density at the nuclei.

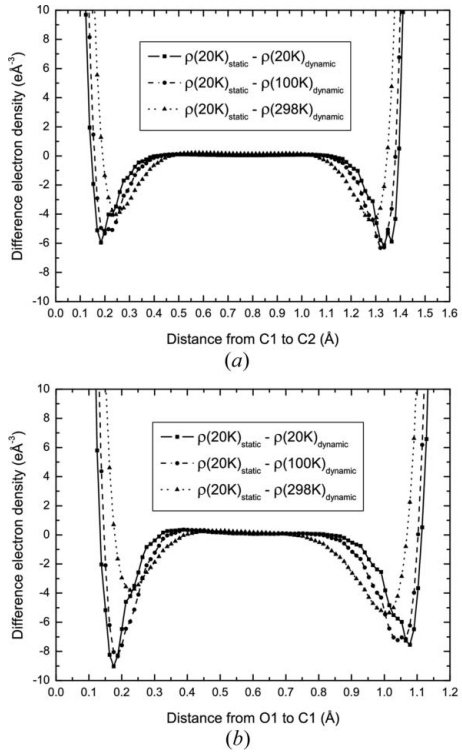

Figure 6
Differences between static MP density at 20 K and dynamic MP densities at different temperatures for D,L-serine plotted along bond paths. (*a*) Difference densities along the bond path C1—C2. (*b*) Difference densities along the bond path O1—C1.

5. Dynamic *versus* static electron densities

5.1. Atomic maxima

Static electron densities possess local maxima of very large values at the positions of the nuclei. Thermal motion of any magnitude leads to smearing of this density, resulting in much lower values at corresponding local maxima of the dynamic charge density (Stewart, 1968). The major difference between dynamic and static densities can thus be expected at positions close to the locations of the atoms.

Topological analyses of the dynamic electron densities of α-glycine and D,L-serine unveil local maxima at positions of all non-H atoms, which closely match the positions of local maxima in the corresponding static electron densities. Non-atomic maxima have not been found. Local maxima in the dynamic electron densities are not obtained for most H atoms. This feature has been explained previously by the very small values of the dynamic electron densities of H atoms, which, even at their maximum values, are smaller than the densities at distances of $\sim$1 Å from the positions of non-H atoms to which the H atoms are covalently bonded (Hofmann *et al.*, 2007).

Density values at local maxima of dynamic electron densities are much smaller than density values at corresponding maxima of static densities (Figs. 4, 5 and 6). This feature indicates that zero-point vibrations are sufficient for smearing of the high magnitude of the static electron densities near the nuclei. Thermal smearing beyond zero-point vibrations leads to a further large decrease of the density values at local maxima (Fig. 5).

5.2. Electron densities outside local maxima

The low-density regions of the static and dynamic electron densities can hardly be distinguished from each other on the basis of a global consideration of the electron-density distributions, as is apparent from contour plots of the densities on the main skeletal planes (O1—O2—C1—C2—N) of α-glycine and D,L-serine (Figs. 7 and 8). Especially for the electron densities at 20 K, the dynamic deformation densities and corresponding static deformation densities exhibit the same features, while for increasing temperature, the dynamic deformation density becomes progressively flatter (Figs. 7*b*, 7*d*, and 8*b*, 8*d*, 8*f*, 8*h*).

These observations are corroborated by a quantitative analysis of the topological properties of dynamic electron densities. BCPs are found for all covalent bonds and all hydrogen bonds at positions expected on the basis of the BCPs in the static electron densities, which indicates a successful calculation of the dynamic electron densities (Coppens, 1997). Values of the dynamic densities at BCPs are only weakly dependent on temperature, and they are close to the corresponding values of the static densities (Tables 4, 5, 6, 7).

For covalent bonds, dynamic electron densities at BCPs are systematically smaller than corresponding static electron densities, with an average difference of 0.06 e Å^{-3} at 20 K,

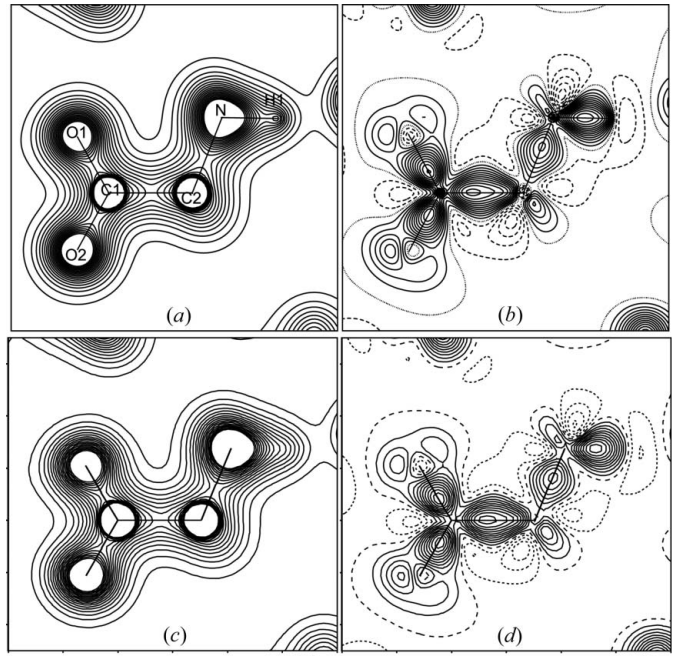

Figure 7
C1—C2—N plane of (*a*), (*c*) the electron density, and (*b*), (*d*) the deformation density of α-glycine. (*a*), (*b*) present the static density, and (*c*), (*d*) give the dynamic density for T = 23 K. Contours are at 0.2 up to 3.6 e Å^{-3} for densities and at an interval of 0.05 e Å^{-3} for deformation densities. Positive density values are indicated by solid lines; negative values by dashed lines; and the zero contour by either dotted or long dashed lines.

increasing to 0.08 e Å^{-3} at 100 K and 0.09 e Å^{-3} at 298 K (Table 6). At the lower temperatures, these differences cannot be explained by the small differences in the positions of the BCPs in dynamic and static electron densities: the maximum distance between positions of corresponding BCPs is 0.01 Å at 20 K and 0.02 Å at 100 K (supplementary material). The distance between positions of corresponding BCPs at 298 K (maximum distance of 0.08 Å for a C—O bond) partly

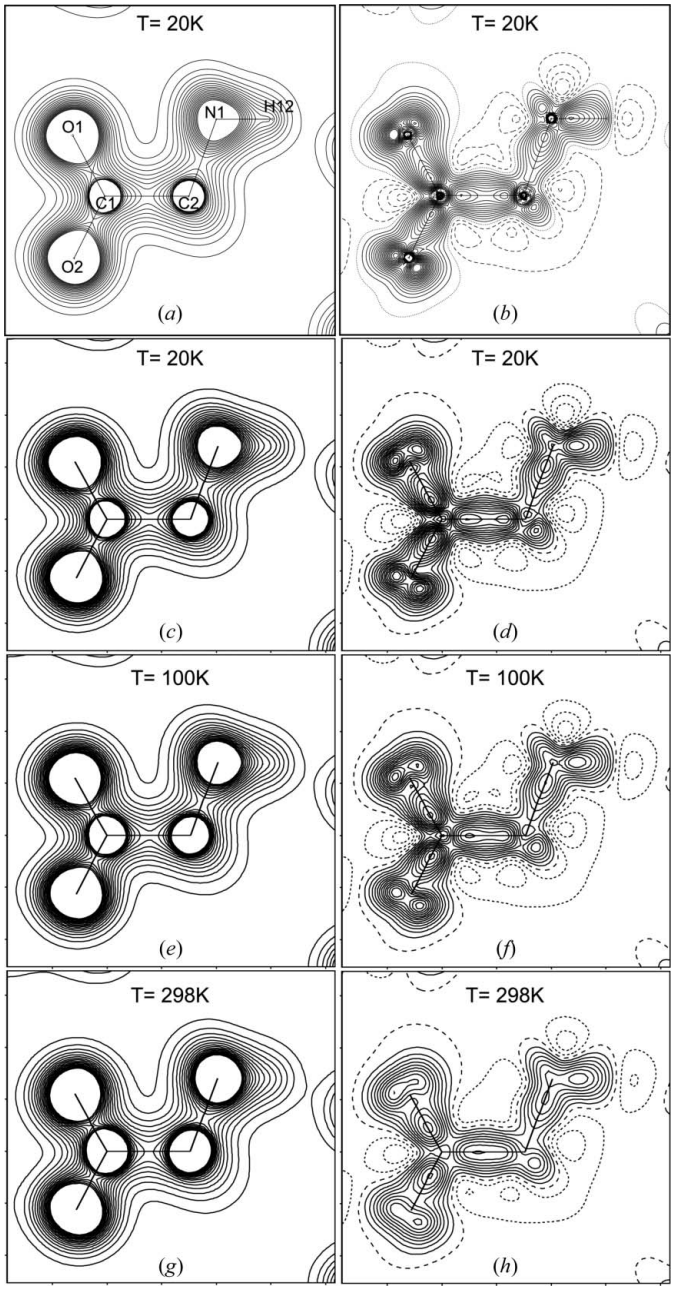

Figure 8
C1—C2—N plane of (*a*), (*c*), (*e*), (*g*) the electron density, and (*b*), (*d*), (*f*), (*h*) the deformation density of D,L-serine at different temperatures. (*a*), (*b*) present the static density, and (*c*)–(*h*) give the dynamic density. Contours are at 0.2 up to 3.6 e Å^{-3} for densities and at an interval of 0.05 e Å^{-3} for deformation densities. Positive density values are indicated by solid lines; negative values by dashed lines; and the zero contour by either dotted or long dashed lines.

Table 4
Electron densities (e Å^{-3}; first line) and Laplacians (e Å^{-5}; second line) at the BCPs of covalent bonds of the dynamic IAM density, the dynamic MP density and the static MP density of α-glycine.

	Dynamic		Static
Bond	IAM	MP	MP
C1—O1	2.043	2.701	2.770
	12.37	−19.44	−36.57
C1—O2	2.017	2.648	2.733
	6.81	−23.61	−35.07
C1—C2	1.184	1.698	1.735
	0.25	−13.28	−12.80
C2—N	1.401	1.657	1.691
	1.87	−10.21	−10.42

Table 5
Electron densities (e Å^{-3}; first line) and Laplacians (e Å^{-5}; second line) at the BCPs of hydrogen bonds of the dynamic IAM electron density, the dynamic MP electron density and the static MP electron density of α-glycine.

	Dynamic		Static
Bond	IAM	MP	MP
O1···H1—N	0.338	0.289	0.283
	2.57	2.51	2.68
O2···H2—N	0.294	0.249	0.240
	3.06	2.77	2.29
O2···H3—N	0.194	0.158	0.151
	1.95	1.61	1.51
O1···H3—N		0.072	0.065
		1.29	1.24
O1···H4—C2	0.095	0.070	0.063
	1.09	1.04	0.95
O2···H4—C2	0.103	0.077	0.070
	1.14	1.13	1.09

accounts for the difference in density values at BCPs between dynamic and static MP electron densities, although a general trend cannot be established. These differences in values of electron densities can be compared to the much larger differences between density values at corresponding BCPs of dynamic IAM and dynamic MP electron densities, which amount to 0.4–0.6 e Å^{-3} (Tables 4 and 6). In general, differences between dynamic and static MP electron densities are more pronounced for polar-covalent C—O bonds, and to a lesser extent for C—N bonds, than for symmetric C—C bonds.

Hydrogen bonds possess much smaller electron densities at their BCPs than covalent bonds do. For the compounds studied, electron densities at BCPs of hydrogen bonds are between 0.06 and 0.31 e Å^{-3} (Tables 5 and 7). For hydrogen bonds in corresponding BCPs, the value of the static MP electron density is slightly smaller than the value of the dynamic MP electron density, which is then much smaller than the value of the dynamic IAM electron density. Although absolute differences are small, relative differences between values of static and dynamic electron densities at corresponding BCPs of hydrogen bonds are equal to or larger than those of covalent bonds. Essential features of the static deformation densities of hydrogen bonds are preserved in the dynamic deformation densities (Fig. 9), while features become flatter on increasing temperature.

Table 6
Electron densities (e Å^{-3}; first line) and Laplacians (e Å^{-5}; second line) at the BCPs of covalent bonds of the dynamic IAM electron density, the dynamic MP electron density and the static MP electron density of D,L-serine at three different temperatures.

	20 K			100 K			298 K		
	Dynamic		Static	Dynamic		Static	Dynamic		Static
Bond	IAM	MP	MP	IAM	MP	MP	IAM	MP	MP
C1—O1	2.062	2.723	2.810	2.106	2.716	2.814	2.319	2.793	2.831
	8.19	−23.40	−32.18	15.70	−12.04	−32.30	25.50	8.03	−32.82
C1—O2	2.025	2.693	2.791	2.050	2.661	2.795	2.191	2.648	2.814
	9.77	−24.15	−35.32	16.84	−13.22	−35.50	27.78	8.90	−36.28
C3—O3	1.566	1.807	1.869	1.582	1.795	1.874	1.731	1.874	1.888
	6.12	−9.02	−16.64	9.74	−2.16	−16.80	26.10	18.63	−17.30
C1—C2	1.174	1.669	1.710	1.174	1.649	1.713	1.166	1.568	1.716
	1.01	−11.23	−11.77	0.60	−11.25	−11.84	0.25	−10.09	−11.87
C2—C3	1.201	1.684	1.726	1.202	1.662	1.730	1.201	1.584	1.735
	−0.63	−13.60	−12.29	−1.00	−13.41	−12.36	−0.69	−11.10	−12.46
C2—N1	1.395	1.664	1.684	1.408	1.661	1.686	1.458	1.669	1.690
	0.28	−12.20	−10.06	0.085	−11.19	−10.09	4.64	−2.62	−10.17

Table 7
Electron densities (e Å^{-3}; first line) and Laplacians (e Å^{-5}; second line) at the BCPs of hydrogen bonds of the dynamic IAM electron density, the dynamic MP electron density and the static MP electron density of D,L-serine at three different temperatures.

	20 K			100 K			298 K		
	Dynamic		Static	Dynamic		Static	Dynamic		Static
Bond	IAM	MP	MP	IAM	MP	MP	IAM	MP	MP
O1···H4—O3	0.376	0.279	0.258	0.381	0.288	0.259	0.386	0.305	0.252
	2.87	3.91	4.29	2.74	3.79	4.31	2.03	3.00	4.20
O3···H11—N1	0.324	0.237	0.219	0.322	0.238	0.217	0.324	0.248	0.209
	3.16	4.10	3.89	3.10	4.02	3.83	2.77	3.71	3.71
O2···H12—N1	0.304	0.218	0.200	0.310	0.224	0.200	0.310	0.233	0.187
	2.99	3.71	3.47	2.97	3.74	3.51	2.62	3.40	3.29
O2···H13—N1	0.288	0.202	0.185	0.291	0.207	0.183	0.298	0.221	0.175
	3.09	3.84	3.42	3.04	3.81	3.40	2.78	3.58	3.27
O1···H2—C2	0.137	0.086	0.075	0.141	0.090	0.075	0.155	0.104	0.074
	1.87	1.97	1.53	1.90	2.03	1.53	1.94	2.19	1.52

Dynamic effects on electron densities can be rationalized as follows. In principle, thermal smearing leads to much smaller values of dynamic electron densities at the atomic maxima than of static electron densities at corresponding atomic maxima (§5.1). In regions of lowest values of static electron densities, thermal smearing must lead to larger values in the dynamic electron densities, since the total number of electrons is constant, and only their distribution over the unit cell is modified by thermal smearing. At points with density values between highest and lowest values, a general trend cannot be established on going from static to dynamic electron densities. The different values of static and dynamic electron densities depend on the value of the density, the temperature, the distances to and the types of the atoms.

This is illustrated by comparing dynamic electron densities and corresponding static electron densities along bond paths between two atoms. Maximum differences are found at the local maxima (at the positions of the atoms). After an initial decrease of this difference on increasing distance to the atom, two points of intersection are found where static and dynamic electron densities are equal to each other, before reaching the BCP (Figs. 4, 5 and 6). The locations of these points of intersection depend on temperature as well as on the type of atoms comprising the bond, with a largest shift of 0.12 Å for a C—O bond of D,L-serine.

5.3. Topological descriptors beyond electron densities

While static and dynamic electron densities possess comparable values at their BCPs, this is not true for the second derivatives of the electron densities.[2] At BCPs, the Hessian matrix of second derivatives has two negative eigenvalues corresponding to directions perpendicular to the bond path, and one positive eigenvalue corresponding to the direction along the bond path. For C—C and C—N bonds at 20 K (zero-point vibrations), the magnitudes of the three curvatures are smaller for dynamic than for static densities (Tables 8 and 9), indicating that near the BCPs of these bond types dynamic electron densities are less steep than static electron densities, in agreement with a naive understanding of thermal smearing. The largest effect of zero-point vibrations is for C—O bonds, for which the magnitudes of the two negative eigenvalues decrease, but for which the positive eigenvalues increase, indicating that the curvature at BCPs along the bond paths of C—O bonds is larger in dynamic electron densities than in

[2] The first derivatives or gradients of the electron density are zero at BCPs.

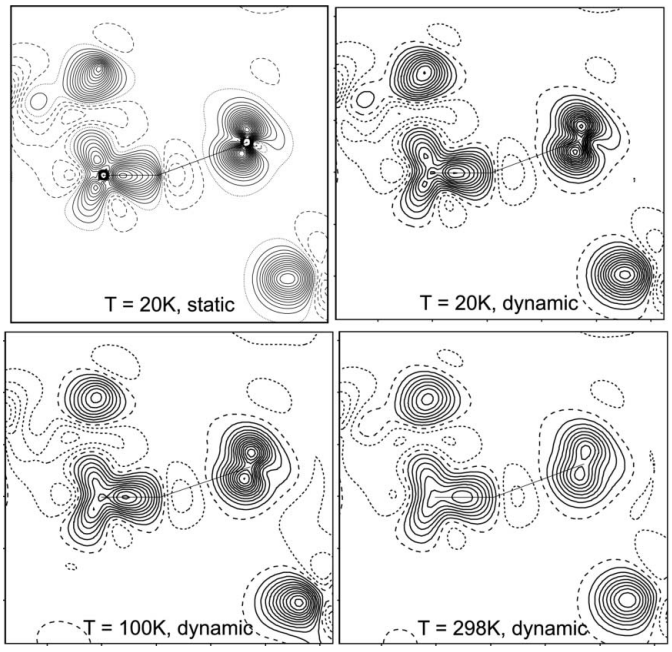

Figure 9
Static and dynamic deformation densities of D,L-serine in the plane defined by N1, H12 and O2, showing the N1—H12···O2 hydrogen bond. The contour interval is 0.05 e Å^{-3}. Positive density values are indicated by solid lines; negative values by dashed lines; and the zero contour by either dotted or long dashed lines.

Table 8
Principal curvatures (λ_1, λ_2 and λ_3) and Laplacians (e Å^{-5}) at BCPs of the static MP electron density (first line) and the dynamic MP electron density (second line) of α-glycine at 23 K.

Bond	λ_1	λ_2	λ_3	$\nabla^2\rho$
C1—O1	−25.78	−23.99	13.20	−36.57
	−23.13	−22.47	26.16	−19.44
C1—O2	−26.24	−22.02	13.18	−35.07
	−24.35	−20.45	21.18	−23.61
C1—C2	−13.28	−11.28	11.75	−12.80
	−12.85	−10.58	10.16	−13.28
C2—N	−12.26	−12.00	13.83	−10.42
	−11.44	−11.11	12.34	−10.21
O1···H1—N	−1.73	−1.69	6.09	2.68
	−1.72	−1.63	5.86	2.51
O2···H2—N	−1.39	−1.37	5.05	2.29
	−1.36	−1.30	5.43	2.77
O2···H3—N	−0.77	−0.70	2.98	1.51
	−0.80	−0.69	3.10	1.61
O1···H3—N	−0.25	−0.14	1.63	1.24
	−0.27	−0.16	1.72	1.29
O1···H4—C2	−0.23	−0.17	1.34	0.95
	−0.25	−0.20	1.48	1.04
O2···H4—C2	−0.28	−0.21	1.58	1.09
	−0.29	−0.23	1.66	1.13

static electron densities. This effect is magnified at higher temperatures, whereas there is only a moderate temperature dependence of the other curvatures at BCPs of dynamic electron densities (Table 9).

We did not find a simple explanation for these different behaviours, except for the observation that values of the second derivatives will depend on a detailed balance of bond asymmetry, distance of the BCPs to the atoms and anisotropic thermal smearing. The similar values at BCPs of static and dynamic electron densities might have been the reason for interpreting high-density values at midpoints of bonds as indications for covalent bonding (Kato *et al.*, 2005; Nishibori *et al.*, 2007). The present results show that such a simple relation does not hold for dynamic electron densities.

The most interesting single quantity is the Laplacian, which is the sum of the eigenvalues of the Hessian matrix. The opposite trends in the positive and negative curvatures at BCPs of C—O bonds are responsible for the observed large differences between dynamic and static electron densities concerning the values of the Laplacian at BCPs of these bonds (Table 9), while Laplacians at BCPs of the other bonds have comparable values in static and dynamic electron densities at 20 and at 100 K (Tables 4 and 6; Fig. 10). Substantial differences are furthermore found for the Laplacian at the BCPs of the C—N bonds in the dynamic electron density at 298 K.

These differences must be considered in view of the spread of values of Laplacians at BCPs of single-bond types in static electron densities, which have been reported to be as large as 4.7 e Å^{-5} for the C—O bond in the series of amino acids (Mebs *et al.*, 2006). The presently observed difference between 20 K dynamic and static electron densities of ∼12 e Å^{-5} thus will partly reflect the effect of zero-point vibrations on the Laplacians, but it might also indicate a non-perfect modelling of electron densities by the chosen MP model or a non-accurate deconvolution of static density and thermal motion by the MP refinement. Difficulties in accurately describing C—O bonds have been noticed earlier in electron-density studies (Roversi *et al.*, 1996; Benabicha *et al.*, 2000; Birkedal *et al.*, 2004; Netzel & van Smaalen, 2009).

Allowing for an uncertainty of the magnitude observed by Mebs *et al.* (2006), a general trend is observed for covalent bonds, with $\rho_{\rm IAM}^{\rm dynamic}({\rm BCP}) < \rho_{\rm MP}^{\rm dynamic}({\rm BCP}) < \rho_{\rm MP}^{\rm static}({\rm BCP})$ and $\nabla^2\rho_{\rm IAM}^{\rm dynamic}({\rm BCP}) > \nabla^2\rho_{\rm MP}^{\rm dynamic}({\rm BCP}) > \nabla^2\rho_{\rm MP}^{\rm static}({\rm BCP})$.

The different temperature dependence of topological descriptors of different bonds might be related to their different chemical properties. This topic will be the subject of future research. In any case, the present results show that topological properties of dynamic electron densities at very low temperatures (20 K) provide at least a semi-quantitative estimate for the values expected for static densities.

Hydrogen bonds possess Laplacians and eigenvalues of the Hessian matrix of similar values in the static electron density and the dynamic electron densities at all three temperatures. A possible explanation is that electron densities around BCPs of hydrogen bonds are so small that they exhibit only small variations with position, with increasingly small effects of thermal smearing (Tables 5, 7).

Table 9
Principal curvatures (λ_1, λ_2 and λ_3) and Laplacians (e Å^{-5}) at BCPs of electron densities of D,L-serine at temperatures of 20, 100 and 298 K.

Values are given for the static MP density at 20 K (first line), the dynamic MP density at 20 K (second line), the dynamic MP density at 100 K (third line) and the dynamic MP density at 298 K (fourth line).

Bonds	λ_1	λ_2	λ_3	$\nabla^2\rho$
C1—O1	−26.84	−24.68	19.34	−32.18
	−26.98	−24.26	27.84	−23.40
	−26.40	−24.15	38.51	−12.04
	−25.28	−24.15	57.46	8.03
C1—O2	−28.00	−25.38	18.06	−35.32
	−27.72	−22.62	26.19	−24.15
	−26.97	−21.50	35.25	−13.22
	−25.25	−18.88	53.03	8.90
C3—O3	−16.12	−15.54	15.02	−16.64
	−13.82	−12.44	17.24	−9.02
	−13.28	−12.04	23.16	−2.16
	−13.62	−12.43	44.69	18.63
C1—C2	−13.32	−12.43	13.97	−11.77
	−12.94	−10.84	12.55	−11.23
	−12.49	−10.34	11.58	−11.25
	−10.90	−8.72	9.53	−10.09
C2—C3	−13.17	−12.61	13.49	−12.29
	−13.42	−11.17	10.99	−13.60
	−12.81	−10.64	10.04	−13.41
	−11.00	−9.03	8.92	−11.10
C2—N1	−13.85	−12.47	16.26	−10.06
	−15.01	−10.85	13.66	−12.20
	−14.61	−10.58	13.99	−11.19
	−14.02	−10.37	21.76	−2.63
O1···H4—O3	−1.42	−1.40	7.11	4.29
	−1.75	−1.35	7.01	3.91
	−1.79	−1.38	6.97	3.79
	−1.77	−1.38	6.14	3.00
O3···H11—N1	−1.09	−1.08	6.05	3.89
	−1.24	−1.05	6.40	4.10
	−1.23	−1.04	6.30	4.02
	−1.25	−1.02	5.98	3.71
O2···H12—N1	−1.02	−0.97	5.46	3.47
	−1.13	−1.00	5.83	3.71
	−1.16	−1.01	5.91	3.74
	−1.17	−0.99	5.57	3.40
O2···H13—N1	−0.93	−0.90	5.25	3.42
	−1.05	−0.91	5.79	3.84
	−1.07	−0.92	5.80	3.81
	−1.10	−0.95	5.63	3.58
O1···H2—C2	−0.28	−0.27	2.07	1.53
	−0.33	−0.27	2.56	1.97
	−0.34	−0.29	2.66	2.03
	−0.41	−0.35	2.95	2.19

Thermal smearing has been found to have only a small effect on the number of electrons in each atomic basin (Table 10). This is explained by the fact that small shifts of the boundaries of the atomic basins take place in low-density regions and thus hardly affect integral properties, like the number of electrons. Ionic charges can thus be extracted from dynamic densities with values nearly equal to the ionic charges based on static densities.

Table 10
Charges from the basin integration for all atoms in D,L-serine.

H atoms in brackets are included in the atomic basin of the corresponding parent atom.

Atom	Static MP model (20 K)	Dynamic MP model (20 K)	Dynamic MP model (100 K)	Dynamic MP model (298 K)
C3(+H31+H32)	7.7267	7.6988	7.6945	7.7139
C2(+H2)	6.5763	6.5798	6.5820	6.6185
O2	8.8825	8.9041	8.8908	8.8214
N1(+H11+H12+H13)	9.7152	9.7220	9.7223	9.6977
O3(+H4)	9.5142	9.5335	9.5350	9.4935
C1	4.6216	4.5747	4.5995	4.7668
O1	8.9705	8.9872	8.9759	8.8882
Total charge	−0.0070	0.0000	0.0000	0.0000
H2	0.9174	0.7901	0.7046	
H4	0.3836			
H11	0.5238			
H12	0.5267			
H13	0.5296			
H31	0.9596	0.8283		
H32	0.9590	0.7901		

6. Conclusions

We have demonstrated that dynamic electron densities of MP and IAM models can be successfully constructed by inverse Fourier transform of the model structure factors, employing the method of FFT. For organic compounds, an electron density sampled on a grid of mesh 0.04 Å or smaller guarantees a dynamic electron density free of series-termination effects. This mesh corresponds to a resolution better than $[\sin(\theta)/\lambda]_{\max} \simeq 6$ Å^{-1} in reciprocal space (§4). Employing the same method of interpolation as in *XD2006* for calculating the spherical parts of atomic scattering factors, we have demonstrated that the software *PRIOR* accurately computes the structure factors of an MP model. Exact calculation of atomic scattering factors leads to significantly different values of the structure factors, and thus is the preferred procedure (Appendix *A*).

The absence of series-termination effects is demonstrated by a topological analysis of the dynamic electron densities, which exhibit features similar to static electron densities, including the occurrence of atomic maxima and BCPs at expected positions, and the absence of non-atomic maxima. An exception is H atoms, which do not necessarily lead to a local maximum in the dynamic electron density, a feature that is due to the very small contribution to dynamic densities of the thermally smeared maxima of H atoms (Hofmann *et al.*, 2007). Integral properties over atomic basins, like ionic charges, are nearly equal between static and dynamic densities (§5.2).

Major differences between static and dynamic electron densities are already found for zero-point vibrations, as has become apparent from the analysis of dynamic electron densities at a temperature of ∼20 K. Values at atomic maxima

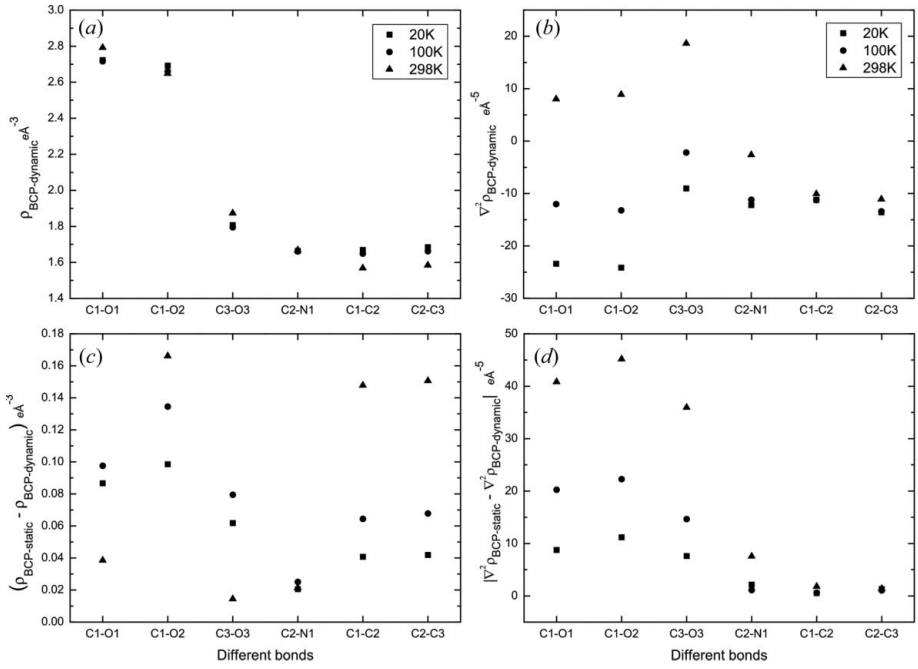

Figure 10
Topological properties for covalent bonds from dynamic densities of the MP model and the differences with corresponding static properties. (*a*) ρ_{BCP} from dynamic MP densities at different temperatures. (*b*) $\nabla^2\rho_{BCP}$ from dynamic MP densities at different temperatures. (*c*) Differences between ρ_{BCP} from static and dynamic densities of the MP model at different temperatures. (*d*) Absolute values of differences between $\nabla^2\rho_{BCP}$ from static densities and dynamic densities of the MP model at different temperatures.

are much smaller in dynamic electron densities than in static electron densities, in agreement with the general understanding of thermal smearing. The different values of topological descriptors at BCPs of covalent bonds in dynamic and static electron densities cannot be predicted with simple arguments, but seem to be the result of a delicate balance between the magnitude of the electron density, distances to the atoms and anisotropic thermal smearing.

In general, dynamic electron densities have slightly smaller density values at BCPs than static electron densities have, but rather larger differences have been found for Laplacians of polar covalent bonds, with differences of increasing magnitude for increasing polarity and for dynamic densities of increasing temperature (§5.2). Nevertheless, at temperatures below 100 K, and especially at ∼20 K, topological properties at BCPs of dynamic electron densities provide at least a semi-quantitative estimate of the topological properties of static electron densities. This shows that chemical bonding can approximately be described by topological properties of low-temperature dynamic densities, although the QTAIM has not been developed for dynamic densities.

Topological properties of different bonds of the same type (the same chemical environment) have been found to be similar in static electron densities (Mebs *et al.*, 2006). Here we have found that this property holds true for dynamic electron densities too.

Differences in values of Laplacians at BCPs in dynamic electron densities at different temperatures, along with the temperature dependencies of other descriptors not considered here, might be helpful in understanding the chemical properties of compounds. This is the subject of future research. Particularly useful would be a theory relating topological properties of dynamic electron densities to chemical properties at finite temperatures.

Hydrogen bonds have relatively small density values at their BCPs in both static and dynamic electron densities of either the MP model or the IAM. Accordingly, electron densities are only weakly varying in these regions. This observation explains why both the density values and the Laplacians at BCPs of a hydrogen bond are of similar magnitude in static and dynamic electron densities at all three temperatures, while these quantities have again similar values between dynamic MP electron densities and dynamic IAM electron densities. These observations explain that one might employ static or dynamic IAM densities instead of the true MP densities for describing the properties of hydrogen bonds (Spackman, 1999; Downs *et al.*, 2002). However, it has been shown that the observed dependencies of the topological properties at BCPs on the length of the hydrogen bond follow different trends in the cases of IAM and MP electron densities (Espinosa *et al.*, 1999; Netzel & van Smaalen, 2009). Therefore, the true electron densities cannot be replaced by IAM electron densities.

APPENDIX *A*
The computer program *PRIOR*

The modified computer program *PRIOR* (van Smaalen *et al.*, 2003) reads an instruction file followed by reading of the multipole parameters from a crystallographic information file (CIF) (Hall & McMahon, 2006). The CIF standard, which is followed by many refinement programs, specifies that values of parameters should be given up to one or two significant digits, followed by the one or two digits of the standard uncertainty (s.u.) enclosed in brackets. A quantity computed from these parameters can be more accurate than suggested by the s.u.'s, if high correlations exist between the parameters.[3] This is the situation for the MP model, which usually suffers from high correlations between, and large s.u.'s of, parameters, but which provides an accurate description of the electron density. Since the purpose of our procedure is to compute a dynamic electron density which exactly corresponds to the structure models presented by computer programs like *XD*

[3] For an example in a different context see Röttger *et al.* (2012).

and *MOPRO* (Volkov *et al.*, 2006; Jelsch *et al.*, 2005), we need values of the MP parameters with more digits than usually contained in the CIF files produced by these computer programs. This can be achieved by editing the CIF files. Alternatively, the output file of *XD2006* contains values with six significant digits for all parameters. Therefore, an option has been included in *PRIOR* for reading the values of the MP parameters from the output file XD_LSM.OUT of *XD2006*.

The present implementation of the computation of structure factors of the MP model employs double-precision variables for all real and complex numbers. This turned out to be necessary in view of the huge dynamic range of values of structure factors when they are incorporated up to resolutions of $\sim$6 Å^{-1}.

The computation of structure factors in *PRIOR* has been validated by comparing the computed values with the values of the real and imaginary parts of $F(\mathbf{H})$ as computed in *XD2006*. Since the structure factors for inverse Fourier transform should not contain contributions of anomalous scattering nor corrections for extinction or scale factor, a special version of *XD2006* has been kindly provided by L. J. Farrugia (Farrugia, 2012), which produces an additional output file containing the real and imaginary parts of $F(\mathbf{H})$ with six significant digits. The *XD2006* software computes the spherical parts of the atomic scattering factors by interpolation of a previously computed table of values {step size of 0.1 Å^{-1} in [sin(θ)/λ]}. The procedure of interpolation has been kindly provided by P. Macchi (Macchi, 2012) and it has been implemented in *PRIOR*. For the list of experimental reflections (which are contained in the output of *XD2006*) a maximum relative difference of less than 10^{-5} has been found in the structure factors as calculated by *XD2006* and *PRIOR*, respectively. In view of the available six significant digits for both MP parameters and structure factors from *XD*, this discrepancy is within the expected range, and it is concluded that the computation of structure factors of the MP model is performed correctly in *PRIOR*.

PRIOR also contains the option of exact computation of the atomic scattering factors for each reflection. For this case, a maximum relative difference between *XD2006* and *PRIOR* has been found of 0.2% for a model composed of a single carbon atom, and of 14% for a weak reflection of α-glycine. These discrepancies reflect the error made by the interpolation procedure of computing atomic form factors. However, for most reflections the difference is smaller, because errors may cancel each other and because the deviation of interpolated values from true values of the atomic form factors will be small for scattering vectors with a length close to the points used for the procedure of interpolation. A comparison of the two different calculations as performed with *PRIOR* showed that the exact computation needs about four times more CPU time than the calculations with interpolated atomic form factors. In view of the increased computational power that is presently available as compared to 15 years ago, the exact computation of atomic form factors seems to be the advisable procedure.

We are grateful to R. Destro for providing the diffraction data of α-glycine, and to B. Dittrich for providing the diffraction data of D,L-serine. Financial support has been obtained from the German Science Foundation (DFG).

References

Bader, R. F. W. (1990). *Atoms in Molecules – a Quantum Theory*. New York: Oxford University Press.

Benabicha, F., Pichon-Pesme, V., Jelsch, C., Lecomte, C. & Khmou, A. (2000). *Acta Cryst.* B**56**, 155–165.

Birkedal, H., Madsen, D., Mathiesen, R. H., Knudsen, K., Weber, H.-P., Pattison, P. & Schwarzenbach, D. (2004). *Acta Cryst.* A**60**, 371–381.

Car, R. & Parrinello, M. (1985). *Phys. Rev. Lett.* **55**, 2471–2474.

Cavazzoni, C., Colle, R., Farchioni, R. & Grosso, G. (2002). *Phys. Rev. B*, **66**, 165110.

Coppens, P. (1997). *X-ray Charge Densities and Chemical Bonding*. New York: Oxford University Press.

Coppens, P. & Volkov, A. (2004). *Acta Cryst.* A**60**, 357–364.

Cyrański, M. K., Jezierska, A., Klimentowska, P., Panek, J. J., Zukowska, G. Z. & Sporzyński, A. (2008). *J. Chem. Phys.* **128**, 124512.

Destro, R., Roversi, P., Barzaghi, M. & Marsh, R. E. (2000). *J. Phys. Chem. A*, **104**, 1047–1054.

Dittrich, B., Hübschle, C. B., Holstein, J. J. & Fabbiani, F. P. A. (2009). *J. Appl. Cryst.* **42**, 1110–1121.

Dittrich, B., Hübschle, C. B., Messerschmidt, M., Kalinowski, R., Girnt, D. & Luger, P. (2005). *Acta Cryst.* A**61**, 314–320.

Dittrich, B., Koritsanszky, T. & Luger, P. (2004). *Angew. Chem. Int. Ed.* **43**, 2718–2721.

Downs, R. T., Gibbs, G. V., Boisen, M. B. Jr & Rosso, K. M. (2002). *Phys. Chem. Miner.* **29**, 369–385.

Espinosa, E., Souhassou, M., Lachekar, H. & Lecomte, C. (1999). *Acta Cryst.* B**55**, 563–572.

Farrugia, L. J. (1999). *J. Appl. Cryst.* **32**, 837–838.

Farrugia, L. J. (2012). Personal communication.

Gaigeot, M. P. (2008). *J. Phys. Chem. A*, **112**, 13507–13517.

Hall, S. R. & McMahon, B. (2006). Editors. *International Tables for Crystallography*, Vol. G, 1st online ed. Chester: International Union of Crystallography. [doi:10.1107/97809553602060000107]

Hirshfeld, F. L. (1976). *Acta Cryst.* A**32**, 239–244.

Hofmann, A., Netzel, J. & van Smaalen, S. (2007). *Acta Cryst.* B**63**, 285–295.

Jelsch, C., Guillot, B., Lagoutte, A. & Lecomte, C. (2005). *J. Appl. Cryst.* **38**, 38–54.

Jelsch, C., Pichon-Pesme, V., Lecomte, C. & Aubry, A. (1998). *Acta Cryst.* D**54**, 1306–1318.

Katan, C., Rabiller, P., Lecomte, C., Guezo, M., Oison, V. & Souhassou, M. (2003). *J. Appl. Cryst.* **36**, 65–73.

Kato, K., Ohishi, Y., Takata, M., Nishibori, E., Sakata, M. & Moritomo, Y. (2005). *Phys. Rev. B*, **71**, 012404.

Macchi, P. (2012). Personal communication.

Matta, C. F. & Boyd, R. J. (2007). Editors. *The Quantum Theory of Atoms in Molecules: From Solid State to DNA and Drug Design*. Weinheim: Wiley-VCH.

Mebs, S., Messerschmidt, M. & Luger, P. (2006). *Z. Kristallogr.* **221**, 656–664.

Netzel, J. & van Smaalen, S. (2009). *Acta Cryst.* B**65**, 624–638.

Nijveldt, D. & Vos, A. (1988). *Acta Cryst.* B**44**, 289–296.

Nishibori, E., Sunaoshi, E., Yoshida, A., Aoyagi, S., Kato, K., Takata, M. & Sakata, M. (2007). *Acta Cryst.* A**63**, 43–52.

Palatinus, L., Prathapa, S. J. & van Smaalen, S. (2012). *J. Appl. Cryst.* **45**, 575–580.

Petricek, V., Dusek, M. & Palatinus, L. (2006). *JANA2006. The crystallographic computing system*. Institute of Physics, Czech Academy of Sciences, Prague, Czech Republic.

Rabiller, P., Souhassou, M., Katan, C., Gatti, C. & Lecomte, C. (2004). *J. Phys. Chem. Solids*, **65**, 1951–1955.
Röttger, K., Endriss, A., Ihringer, J., Doyle, S. & Kuhs, W. F. (2012). *Acta Cryst.* B**68**, 91.
Roversi, P., Barzaghi, M., Merati, F. & Destro, R. (1996). *Can. J. Chem.* **74**, 1145–1161.
Roversi, P., Irwin, J. J. & Bricogne, G. (1998). *Acta Cryst.* A**54**, 971–996.
Ruysink, A. F. J. & Vos, A. (1974). *Acta Cryst.* A**30**, 497–502.
Sheldrick, G. M. (2008). *Acta Cryst.* A**64**, 112–122.
Smaalen, S. van, Palatinus, L. & Schneider, M. (2003). *Acta Cryst.* A**59**, 459–469.
Spackman, M. A. (1999). *Chem. Phys. Lett.* **301**, 425–429.
Stevens, E. D., Rys, J. & Coppens, P. (1977). *Acta Cryst.* A**33**, 333–338.
Stewart, R. F. (1968). *Acta Cryst.* A**24**, 497–505.
Stewart, R. F. (1976). *Acta Cryst.* A**32**, 565–574.
Stewart, R. F. & Spackman, M. A. (1983). *VALRAY Users Manual.* Department of Chemistry, Carnegie-Mellon University, Pittsburgh, USA.
Su, Z. & Coppens, P. (1998). *Acta Cryst.* A**54**, 646–652.
Volkov, A., Macchi, P., Farrugia, L. J., Gatti, C., Mallinson, P. R., Richter, T. & Koritsanszky, T. (2006). *XD2006. A computer program package for multipole refinement, topological analysis of charge densities and evaluation of intermolecular energies from experimental or theoretical structure factors.*
Vries, R. Y. de, Briels, W. J. & Feil, D. (1996). *Phys. Rev. Lett.* **77**, 1719–1722.
Vries, R. Y. de, Briels, W. J., Feil, D., te Velde, G. & Baerends, E. J. (1996). *Can. J. Chem.* **74**, 1054–1058.